Ultrafast bandgap narrowing and cohesion loss of photoexcited fused silica

Arshak Tsaturyan, Elena Kachan, Razvan Stoian, Jean-Philippe Colombier

Ultrafast bandgap narrowing and cohesion loss of photoexcited fused silica

Arshak Tsaturyan, Elena Kachan, Razvan Stoian, Jean-Philippe Colombier*

Univ Lyon, UJM-Saint-Etienne, CNRS, IOGS, Laboratoire Hubert Curien UMR5516, F-42023 St-Etienne, France
E-mail: arshak.tsaturyan@univ-st-etienne.fr; jean.philippe.colombier@univ-st-etienne.fr

Keywords: fused silica, laser matter interaction, ultrashort pulses, finite-temperature density functional theory, bandgap

Abstract: Coupling and spatial localization of energy on ultrafast timescales and particularly on the timescale of the excitation pulse in ultrashort laser irradiated dielectric materials are key elements for enabling processing precision beyond the optical limit. Transforming matter on mesoscopic scales facilitates the definition of nanoscale photonic functions in optical glasses. On these timescales quantum interactions induced by charge non-equilibrium become the main channel for energy uptake and transfer as well as for the material structural change. We apply a first-principles model to determine dynamic distortions of energy bands following the rapid increase in the free-carrier population in an amorphous dielectric excited by an ultrashort laser pulse. Fused silica glass is reproduced using a system of $(SiO_4)^{4-}$ tetrahedra, where Density Functional Theory extended to finite-temperature fractional occupation reproduces ground and photoexcited states. Triggered by electronic charge redistribution, a bandgap narrowing of more than 2 eV is shown to occur in fused silica under geometry relaxation. Calculations reveal that the bandgap decrease results from the rearrangement of atoms altering the bonding strength. Despite an atomic movement impacting strongly the structural stability, the observed change of geometry remains limited to 7% of the interatomic distance and occurs on the femtosecond timescale. This structural relaxation is thus expected to take place quasi-instantly following the photon energy flux. Moreover, under intense laser pulse excitation, fused silica loses its stability when an electron temperature of around 2.8 eV is reached. Further increase of the excitation energy leads to the collapse of both structure and bandgap.

I. Introduction

The interaction of femtosecond laser pulses with a wide-bandgap dielectric and its capability to localize energy within its volume is the backbone of emerging technologies of 3D refractive index engineering and of efficient fabrication of photonic chips. The developments include, to name only a few, optical guiding systems, sensors, optical memories with high data density, waveguide-based optical information processing, elements of optical quantum computing systems, or 3D photonic crystals.[1-11] Ultrafast laser pulses can also be used to turn a dielectric from an insulating state to a conducting state within few femtoseconds without damaging it, thus offering a dielectric optical switch for signal manipulation at ultrahigh (petahertz) rates.[12, 13]

A recent trend in ultrashort laser processing relies on the use of few-cycle pulses, predicted to achieve ultimate precision, thus preparing a new generation of micro-processing tools.[14, 15] They enable an extended processing control by tuning the interplay between multiphoton excitation and strong field ionization,[16] where the cycling of the laser pulse becomes critical. A lack of knowledge exists however in this domain which only recently started to be filled with the advent of attosecond transient absorption spectroscopy.[17] A better understanding of the ultrafast laser-dielectric interaction will not only enable an optimization of processing parameters but also help to explore new applications such as the creation of extreme non-equilibrium states to control kinetic evolution at the molecular level.

The bandgap is a key parameter in defining the optical response of a dielectric irradiated by an ultrafast laser pulse. Multi-photon, field ionization and avalanche ionization mechanisms depend non-linearly on the bandgap value and its even slight modification during the laser pulse can strongly alter the photoexcitation process. Several processes can affect the band structure in antagonistic ways. First of all, the bandgap is expected to transiently increase in response to the ponderomotive energy of the oscillating field.[18, 19] The strong electric field in turn can bend the bands and provoke an effective decrease of the bandgap through the dynamical Franz-Keldysh effect.[16, 17, 20] Another high-field effect consists in Stark splitting of degenerate energy levels also leading to bandgap narrowing.[21] Moreover, the bandgap changes due to the band renormalization induced by strong electronic excitations as already observed in semiconductors,[22, 23] and it can happen on attosecond time scale during the laser pulse.[24] In wide-bandgap dielectrics excited at high laser intensities, such band renormalization could also play an important role; for example, a significant bandgap shrinkage on the order of 3 eV was hypothesized to account for the onset of nonlinear parametric amplification in sapphire and fused silica.[25] The bandgap obviously depends on atomic arrangement and thus is sensitive for

example to high pressure[26, 27] and can also decrease in the process of laser-induced structural transformations.[28]

In this work, we model fused silica under strong laser-induced electronic excitations. We show using Density Functional Theory that excited electron charge redistribution is strong enough to affect the ionic positions, leading to unexpectedly fast bond elongation on a femtosecond timescale. As a result, a bandgap gradual decrease as a function of the electron excitation degree is observed with a total cohesion loss above excited electron density of 10^{22} cm^{-3}.

Fused silica is a glass consisting of silica (SiO_2) in amorphous form exhibiting various structural variations since the topological arrangement of the orthosilicate $(SiO_4)^{4-}$ anion is not unique. Previous atomic-scale modeling efforts focused however mostly on ultrafast laser excitations in crystalline SiO_2 using periodic boundary conditions.[29] In this work, we propose an original molecular cluster model reproducing the behavior of amorphous silica with a high density of excited electrons. The cluster model approach is particularly appropriate to study localized phenomena, such as defects and impurity states, local excitations, or core-level ionization.[30-32] At the molecular level, fused silica is modeled as a discrete-particle-based material consisting of silicon and oxygen atoms mutually bonded via a single covalent polar bond and forming a connected, unstructured network of orthosilicate anions.[33] Since fused silica does not possess any long-range order in its atomic structure, its bulk behavior can be modeled at the molecular level by assuming the existence of a larger (amorphous) unit cell. The molecular cluster method has a great advantage of being computationally simple and low cost compared to large-scale bulk simulations.[34]

The goal of the present paper is thus twofold. The first one is to show the possibility to simulate ultrafast laser excitation in amorphous materials like fused silica by modeling the system at the molecular level. The second one is to unveil the evolution of optical and mechanical properties as soon as strong photoexcitation occurs, explaining the underlying primary mechanism.

II. Computational details

Theoretical calculation of the electronic and atomic structures was performed using DFT and FT-DFT approaches implemented in ORCA program suit.[35] In FT-DFT the electrons are self-consistently smeared over the molecular orbitals according to a Fermi-Dirac distribution:

$$f_i = \frac{1}{\mathrm{e}^{(\varepsilon_i - E_F)/k_B T_e} + 1} \quad (1)$$

where f_i is the fractional occupancy ($0 \leq f_i \leq 1$)), ε_i is the eigen energy of a single-particle state i, E_F is Fermi level of the system, k_B is Boltzmann's constant and T_e is the electron temperature.

The eigen values of all electronic single-particle levels are obtained by solving self-consistently the Kohn-Sham field equations minimizing the electronic free energy.

The fractional orbital density (FOD) is given by a real-space function ρ^{FOD} of position vector r:

$$\rho^{\mathrm{FOD}}(r) = \sum_{i}^{N} (\delta_1 - \delta_2 f_i) \, |\varphi_i(r)|^2, \qquad (2)$$

where φ_i is a wave function of a i^{th} molecular orbital. The constants δ_1 and δ_2 are unity if the energy level of the molecular orbital is lower than E_F while they are 0 and −1, respectively, for levels higher than E_F. The sum runs over all N orbitals of the system. FOD distribution corresponds to the contribution of the "hot" electrons to the electron density. FOD strongly depends on the HOMO – LUMO gap which itself depends almost linearly on the amount of exact HF admixture in chosen hybrid density functional.[36]

The hybrid exchange-correlation functional B3LYP[37] with the value of exact HF admixture varying from 5% to 30% was used. This type of functional is a combination of general gradient approximation (Becke 88 exchange functional and the correlation function of Lee, Yang and Parr) and VWN local spin density approximation. Geometric and electronic optimization of the molecular systems was performed using double and triple zeta split-valence Pople type basis sets.[38]

The DOS were obtained using Gaussian broadening of 0.5 eV width. Given the low local symmetry of the fused silica, all molecular models were computed without any symmetry elements. The molecular volumes needed for mass density calculation were obtained using the GEPOL algorithm as implemented in ORCA conductor-like polarizable continuum model.[39]

RSMD was calculated as follows:

$$\mathrm{RMSD} = \sqrt{\frac{1}{N}\sum_{i=1}^{N} r_i^2}, \quad (3)$$

where r_i is the difference between the position of the i^{th} atom at excited and ground state and N is the number of atoms. Note that only Si and O atoms were considered in this calculation.

The density P and overlap matrix S obtained from electronic population analysis were used to compute the Mulliken gross atomic charges q_A:[40]

$$q_A = Z_A - \sum_{\mu \epsilon A} (\mathbf{P} \cdot \mathbf{S})_{\mu\mu} \quad (4)$$

where Z_A is the charge of atomic nucleus A. The sum runs over atomic orbitals μ of each atom.[41]

The excited electron density as a function of laser pulse fluence (Figure 5) was calculated using Time-Dependent Density Functional Theory (TDDFT) implemented in SALMON code.[42] The calculation details were similar to the ones used for α-quartz in Ref.[43] with TB- mBJ exchange-correlation potential, periodic boundary conditions and an 18-atom unit cell. The following grid parameters were used: $\Delta x = 0.25$ Å, $\Delta y = 0.25$ Å, $\Delta y = 0.10$ Å, 1-as time step and 4^3 k-points. The electric field of the laser pulse E_m inside α-quartz was parallel to z-axis and recalculated from the field in vacuum E_v as $E_m=2E_v/(n+1)$ considering that the change of the refractive index n at the given excitation levels is small.[44]

III. Results and discussions

In silica-based glasses like fused silica, the polyhedron-center atoms are all Si, and each Si atom is surrounded by four O atoms (while each O atom is connected to or bridges two Si atoms) forming a SiO_4 tetrahedron orthosilicate anion. Other kinds of polyhedra and connections may exist. Coexistence of different local arrangements leads to defect formation in the structure, impacting significantly the main physical properties, i.e., bandgap (E_{gap}) value.[45-48]

The various types and number of orthosilicate anions (from 1 to 20) were used to design fused silica. The dangling bonds of the molecular system were saturated by H atoms, a commonly used technique to "embed" clusters of the semiconducting or insulating materials.[49, 50] The position of all atoms including H was fully optimized. The proposed molecular model represents inherently an amorphous material consisting of a 3D network of polyhedral units. The evolution of macroscopic mass density and E_{gap} with the size of the molecular model is shown in **Figure 1.**

The macroscopic density of the studied system increases from 1.8 to 2.3 g cm^{-3} with the cluster size. A cluster with minimum of 10 anions was shown to accurately reproduce mass density and bandgap of fused silica. This cluster with composition $Si_{10}H_{20}O_{30}$ is labeled as $(SiO_2)_{10}$ in the following. The $(SiO_2)_{10}$ density is 2.1 g cm^{-3} which is about 5% lower than the commonly accepted experimental value of 2.2 g cm^{-3} [51] and its bandgap is 9.3 eV also close to the experimental value of 9 eV.[52]

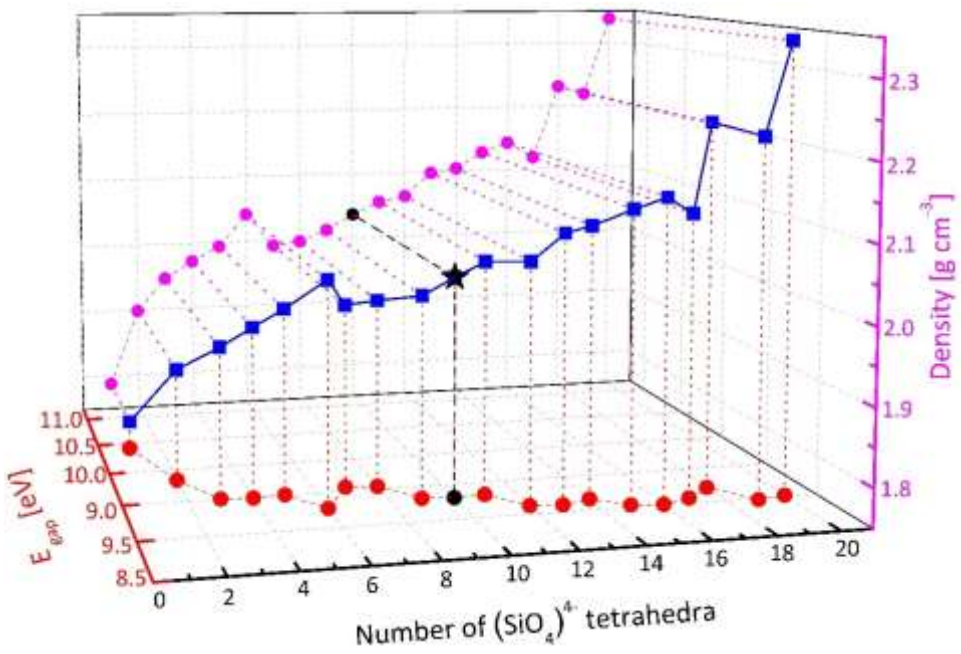

Figure 1. Bandgap (red curve with circles) and mass density (magenta curve with circles) as a function of the number of $(SiO_4)^{4-}$ tetrahedra in the fused silica molecular model. A 3D blue line with squares shows the relation between the three quantities: E_{gap}, number of $(SiO_4)^{4-}$ tetrahedra and density. The black star indicates the size of the molecular model chosen for further analysis.

Note that the energy gap between occupied and empty states in the electronic structure can have different definitions including the bandgap, the highest occupied molecular orbital (HOMO) – lowest unoccupied molecular orbital (LUMO) gap, fundamental gap, and optical gap, with each term carrying a specific meaning.[53] The bandgap shown in Figure 1 corresponds to a HOMO- LUMO gap of the considered molecular system. HOMO-LUMO gap only provides an approximation to the fundamental gap (difference between the ionization potential and electron affinity) or bandgap in solids. The approximation accuracy strongly depends on the specificities of the computational methodology (*ab initio* (HF, post-HF), DFT, GW). For example, in the density-functional theory (DFT) approximation, the HOMO-LUMO gap depends strongly on the type of the exchange-correlation functional and the amount of exact Hartree-Fock (HF) admixture. Fine-tuning the HF admixture in the hybrid functionals with the local DFT exchange improves the accuracy of bandgap calculation in bulk semiconductors and insulators.[54, 55] Therefore, the possibility to improve the accuracy and the smaller demand for computational resources makes DFT more attractive compared to HF, post-HF, and GW approximations for modeling amorphous materials like fused silica. Calculated values of E_{gap}, geometry, and physical parameters, as well as the threshold stability for the $(SiO_2)_{10}$ system obtained by DFT, are given in **Table 1**.

It is well known that the total energy and bandgap has a linear dependency on the amount of exact HF admixture in the hybrid functional.[56, 57] We calculated E_{gap} for different contributions of exact HF admixture (from 5% to 30%) and found that with 30% admixture the bandgap E_{gap} varies from 8.5 to 9.3 eV depending on the basis set, matching very well the experimental value of 9 eV.[52] Pure HF calculation significantly overestimates E_{gap} that reaches 14 eV. The main reason for such deviation is that HF is free of orbital self-interaction, but it is important for small systems where the long-range Coulomb interaction is short-range due to dynamic screening.[58] Consequently, tuning the HF admixture to obtain the correct physical parameters (density and bandgap) and choosing a reasonable size of the molecular system ($(SiO_2)_{10}$ in our case) is a good compromise between accuracy and calculation costs.

Table 1. Bandgap energy E_{gap}, density ρ, geometry parameters, and stability threshold electron temperature T_e of $(SiO_2)_{10}$ calculated using B3LYP functional with 30% of exact HF admixture and different Pople type basis sets (Small - 6-31G, Medium - 6-31G(d) and Large - 6-31+G(d)).

Basis set	Ground state				Excited at the stability threshold				Stability threshold T_e [eV]
	ρ [g cm^{-3}]	Bond length [Å]	Bond angle [°]	E_{gap} [eV]	ρ [g cm^{-3}]	Bond length [Å]	Bond angle [°]	E_{gap} [eV]	
Small	2.00	1.65-1.68	135-168	8.38	1.79	1.76-1.96	140-177	3.17	2.4
Medium	2.04	1.62-1.65	132-165	9.30	1.71	1.74-1.77	152-169	6.84	2.8
Large	2.02	1.62-1.65	135-163	8.52	1.78	1.77-1.81	163-175	6.19	2.9
Experiment	2.19[a]	1.62[b]	144[b]	9.00[c]					

[a)]Reference [51]. [b)]Reference [64]. [c)]Reference [52].

To mimic photo-electronic processes and electronic structure evolution under ultrafast laser irradiation the finite-temperature fractional occupation DFT (FT-DFT) with a hybrid functional and a set of Pople type basis sets was used. This method introduces an electron temperature T_e that applies a Fermi-Dirac-like occupation number smearing over all the orbitals of the system. The used FT-DFT method incorporates self-consistently the effects of thermal electronic excitations and fractionally occupied states that is particularly suited to describe the electronically "hot" subsystem.

Electron temperature increase results in the partial transfer of electrons from occupied to unoccupied states defined by the occupancy evolution. Before excitation, at the ground state corresponding to zero T_e the occupancy of the electron-filled region equals to 1 whereas the unoccupied region has a 0 occupancy. The irradiation by a femtosecond laser pulse, described

as the increase of the electronic temperature, decreases the occupancy of initially filled states and increases the occupancy of empty states describing thermally excited electrons as a result of an ultrafast thermalization process taking place within 10-100 fs.[28] This electronic redistribution modifies the solutions of the Kohn-Sham equations and self-consistent DFT calculations provide the band structure upon thermal excitation.

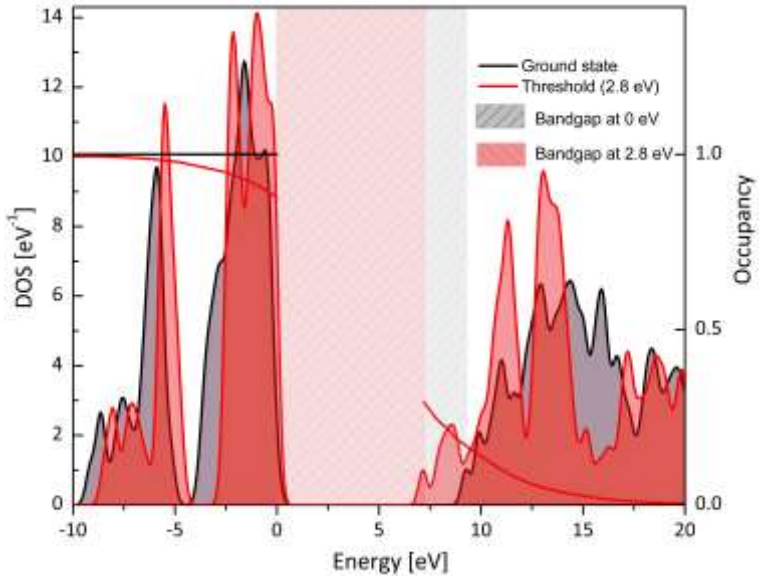

Figure 2. Electronic density of states and Fermi-Dirac occupancy at T_e = 0 eV and T_e = 2.8 eV for $(SiO_2)_{10}$.The bandgap is highlighted in gray with a left sparse pattern (0 eV) and in red with a right sparse pattern (2.8 eV). The stability threshold of the system is around 2.8 eV. At higher electron temperature, Si-O bond breaking occurs. Energy values on x-axis are relative to HOMO level at given temperature.

This is represented by the density of states (DOS) as a function of electron-lattice nonequilibrium as shown in **Figure 2** for the ground-state at T_e = 0 K and for the excited state at T_e = 32350 K (2.8 eV) corresponding to the stability threshold of $(SiO_2)_{10}$. Note that geometry of the molecular model was optimized in both cases. For the temperatures above the stability threshold the bonds start to break. In other words, the distance between Si and O atoms becomes bigger than the sum of covalent radiuses (1.78 Å).

The ground-state DOS matches very well the experimental one[59] and the one obtained from first-principles calculation of bulk fused silica.[60, 61] The edge of the valence band (VB) does not change while the edge of the conduction band (CB) moves to lower energies under the strong laser-induced excitation leading to the bandgap narrowing.

This behavior is characteristic of the screening effect induced at high electron temperature reported previously for metals in a nonequilibrium state.[62] The electron redistribution induces an atomic relaxation that drives a new electronic band structure minimizing the free energy of

the system. Note also that ground-state HOMO (edge of the VB) is localized mainly around O atoms while a significant contribution from Si atoms is observed in LUMO (edge of the CB).[13, 63]

Figure 3 shows the bandgap as a function of electron temperature. E_{gap} decreases monotonously from 9.3 eV down to 7 eV at the stability threshold, thus showing a maximum bandgap decrease of about 2 eV compared to the non-excited state. The bandgap dependence on T_e below the threshold can be fitted by an exponential function (accuracy $R^2 = 0.99$):

$$E_{\text{gap}} = 9.30 - 4.18 \times 10^{-3} e^{2.25 T_e} \quad (5)$$

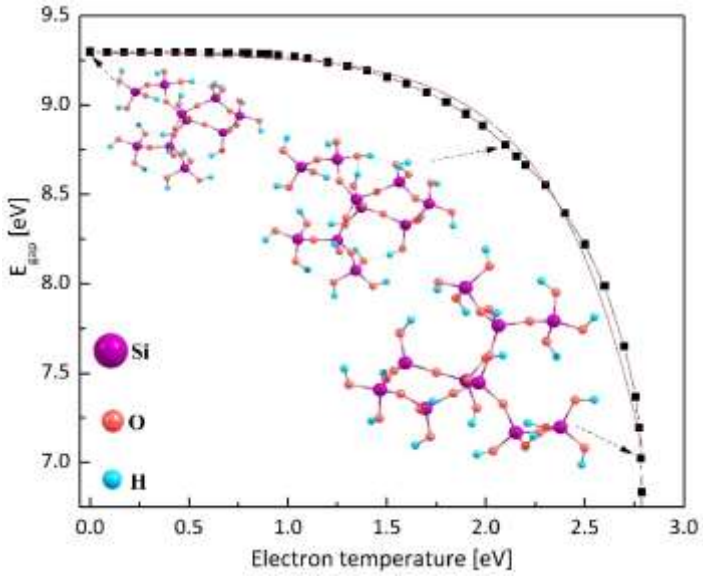

Figure 3. Bandgap energy (E_{gap}) as a function of electron temperature for $(SiO_2)_{10}$ with optimized geometry shown as snapshots for several T_e. Fitting curve (red) is shown.

The mechanical relaxation activated by the system geometry optimization can be unveiled owing to the root mean square atomic displacement (RMSD) as a result of the excitation. The change of RSMD and volume of excited $(SiO_2)_{10}$ up to stability threshold (T_e = 2.8 eV) are shown in **Figure 4**. Before relaxation, the average atomic spacing is in the range of 1.62-1.65 Å for the Si-O nearest neighbors (Table 1 and Figure 4) in perfect agreement with experimental value of 1.62 Å.[64] After relaxation at T_e = 2.8 eV, the bond lengths increase to 1.74-1.77 Å. Such bond elongation leads to 20% of the volume expansion. As the mass of the rapidly heated system remains constant, the volume change triggers a decrease in mass density. If the laser pulse intensity is kept below the critical value triggering the instability, the atomic bonds are preserved and their length increases.

Above T_e = 2.8 eV, the system becomes unstable, and the atom rearrangement provokes bond breaking. The increase of atomic spacing at high T_e clearly indicates that the repulsive force

between the atoms becomes stronger due to the change in the interatomic potential caused by the CB electron generation. The RMSD grows exponentially with the T_e as observed in Figure 4. Its maximum value reach 0.7 Å in response to, as an example, a 15 fs laser pulse delivering a fluence of 3.6 J cm^{-2} (**Figure 5**a can be used to establish the relation between electron temperature and laser pulse parameters).

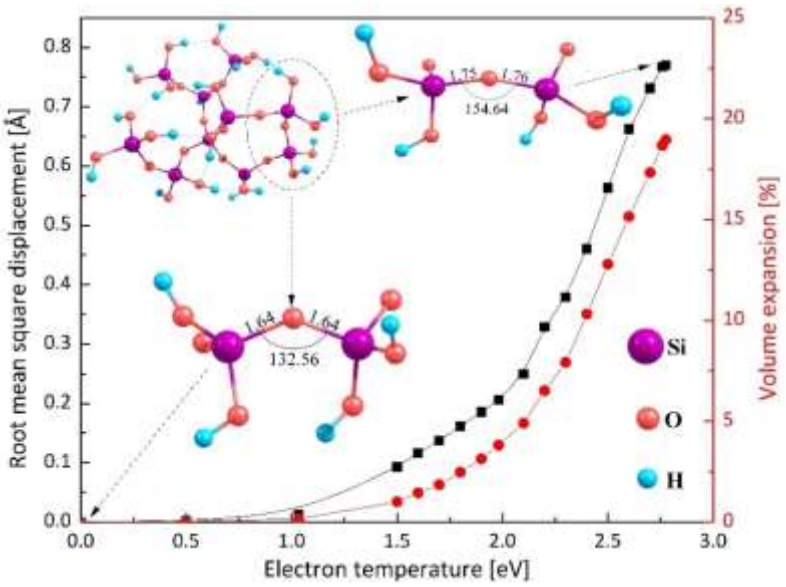

Figure 4. Root mean square atomic displacement (RSMD) as a function of electron temperature for $(SiO_2)_{10}$ (black curve with squares) and volume expansion after geometry optimization (red curve with circles). Insets represent the geometry change (bond angle and length) for two neighboring tetrahedra with maximum RSMD.

To understand why high T_e affects a relaxed atomic configuration of the $(SiO_2)_{10}$, we have performed the fractional occupation number weighted density (FOD) analysis.[40] Figure 5a shows the spatial distribution of FOD around atoms, indicating the localization of the "hot" (excited) electrons. The increase in electron temperature first excites the electrons around O atoms from OH groups then the electrons from bridging oxygen. Finally at T_e > 2.5 eV, the Si electrons are excited. Previously, a similar phenomenon was found under attosecond laser excitation of fused silica where electrons located in the vicinity of the O atoms dominate the nonlinear polarization response, whereas the electron cloud around the Si centers remains largely unaffected.[13]

The Si-O bonds have predominantly polar-covalent character with a minor fraction of ionic type bonding. Redistribution of electronic density in excited system changes the charge of the Si and O atoms changing the ionic fraction in the bond[65]. The ionic bonds are stronger than covalent ones and decrease of the atomic charges leads to the bond weakening. At T_e = 2.8 eV the calculation showed that around 4% of valence electrons in $(SiO_2)_{10}$

($1.4x10^{22}$ electrons per cm^3) were excited from VB to CB. This leads to a change of the atomic charge. The values of Mulliken gross atomic charges as a function of electron temperature are shown in Figure 5(b).[66]

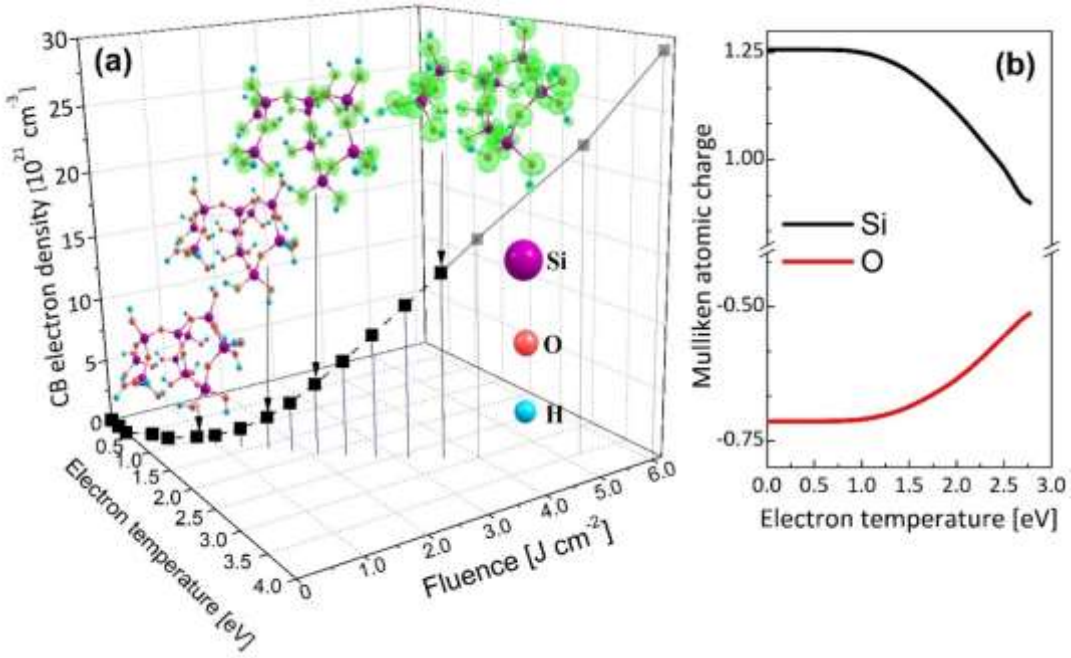

Figure 5. (**a**) Electron density in the CB at different T_e and fluences of a 15 fs (at FWHM) laser pulse. The snapshots of the atomic structure contain isosurfaces of the fractional occupation number weighted density (FOD) (semi-transparent green) at different electron temperatures (1, 1.6, 2 and 2.8 eV) with a contour value $\sigma = 0.067$ Å^{-3}. (**b**) The evolution of the average Mulliken atomic charge of Si (black) and O (red) atoms with T_e.

At the ground state, the atomic charges of Si and O are 1.26 and -0.71, respectively. The redistribution of electron density at $T_e = 2.8$ eV changes the charges of Si and O to 0.90 and -0.51, respectively (Figure 5b). At the same time, the distance between Si and O increases by about 7% (Table 1 and Figure 4). Using Coulomb's law, we estimated a decrease of almost by half of the electrostatic force of attraction between Si and O atoms from the ground to excited states. Such strong attraction weakening leads to the fused silica damage at $T_e > 2.8$ eV. Interestingly, a similar value is reported for other materials.[67, 68] The threshold of nonthermal transition for Al_2O_3 corresponds to $T_e \sim 2.5$ eV.[69] The transition metals destabilization is also expected around $T_e = 2$ eV.[67]

The bond softening and atomic movement along unconventional trajectories as a result of ultrafast electronic redistribution can happen on 10-fs timescale at the fused silica sound velocity for the displacement range reported above (< 1 Å). The bandgap narrowing originated from the atomic rearrangement is thus expected on the same ultrashort timescales. An ultrafast

atomic disordering was also recently shown to influence the bandgap of the laser-excited silicon.[68, 70] Moreover, since amorphous materials like fused silica have a lot of empty space between atoms and crystallinity is absent the atomic relaxation can be realized much easier compared to crystal materials like quartz.

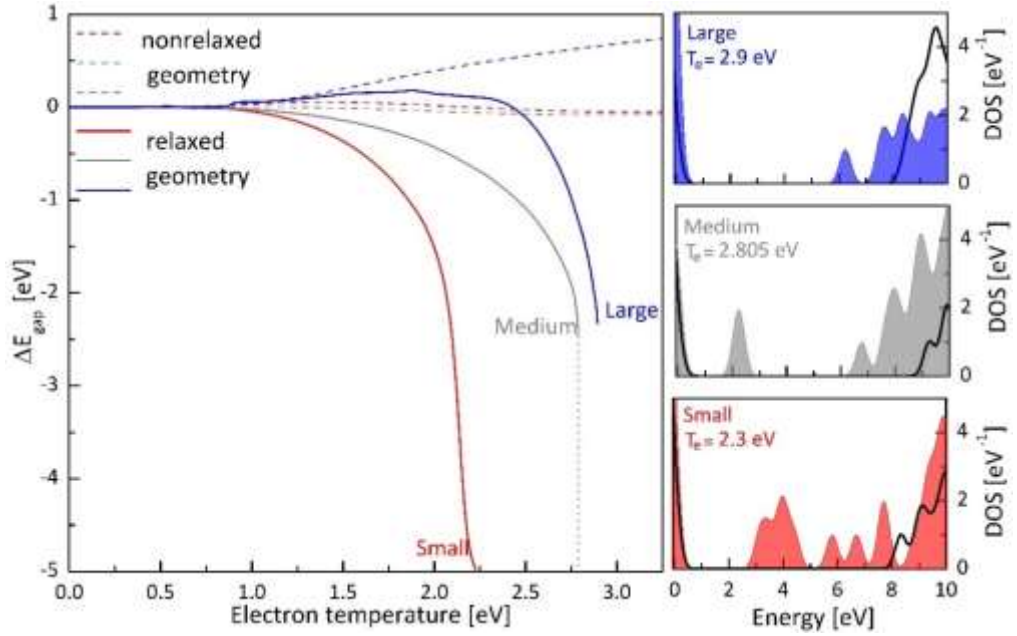

Figure 6. The change of the bandgap relative to the ground state as a function of T_e ($\Delta E_{gap}(T_e) = E_{gap}(0) - E_{gap}(T_e)$) with three different basis sets: red line – Small (6-31G), gray line – Medium (6-31G(d)) and blue line – Large (6-31+G(d)). The changes of the bandgap are shown after geometry optimization (solid) and without geometry optimization (dashed). The gray dot line extrapolates the bandgap collapse after stability threshold. In the second column DOS calculated with three different basis sets at ground state (black solid line) and at relaxed geometry (red – Small, gray – Medium, blue – Large) at T_e = 2.3, 2.805 and 2.9 eV respectively

The bandgap behavior as a function of T_e is shown in **Figure 6** for relaxed and nonrelaxed $(SiO_2)_{10}$. In order to exclude artefacts associated with the choice of the basis set, the calculation with three double zeta split-valence Pople type basis sets (Small – 6-31G, Medium – 6-31G(d), and Large – 6-31+G(d)) were performed. Tests with a higher level of zeta (triple) showed the same trends as for double-zeta basis sets.

For the nonrelaxed $(SiO_2)_{10}$, the E_{gap} does not change in the case of small and medium basis sets. E_{gap} increases by 0.5 eV at T_e = 4 eV for the large basis set. A larger basis set (higher level of zeta, the inclusion of the polarization and diffuse functions) allows for a better representation of the electronic wave function and thus for a more precise adjusting of the electron density and its spatial extent appropriate to a particular molecular environment. With a larger basis set, the electron density becomes more localized around the atomic centers. It can explain the

difference of bandgap behavior between the large basis and smaller ones. An increase of the bandgap was calculated previously for several semiconductors, using DFT with the local density approximation.[71] The observed bandgap increase for a non-relaxed geometry with the large basis set is a pure effect of Fermi-Dirac smearing of electron occupation that depends on the HF admixture to the hybrid exchange-correlation functional B3LYP. After geometry relaxation this effect compensates the bandgap decrease due to atomic rearrangement leading to a total smaller bandgap decrease for a large basis set. For the small and medium basis set the observed bandgap decrease after the geometry relaxation comes purely from atomic rearrangement. Note that the quasiparticle self-consistent GW approximation (known to provide a better estimation for semiconductor bandgaps) shows a bandgap decrease with increasing T_e without relaxation. Thus, a bandgap decrease obtained in this work will in principle add up to the purely electronic bandgap decrease at a higher level of theory (subject of our future work).

The excited electron density redistribution also increases the electronic pressure. If the excitation is too high the thermodynamic stability becomes low, leading to the bond breaking. This process is reflected in the DOS by new peaks formation in the bandgap region. The new peaks appear in the bandgap region of the DOS for medium and small basis sets at a temperature slightly higher than the threshold T_e = 2.805 and 2.3 eV, respectively (Figure 6).

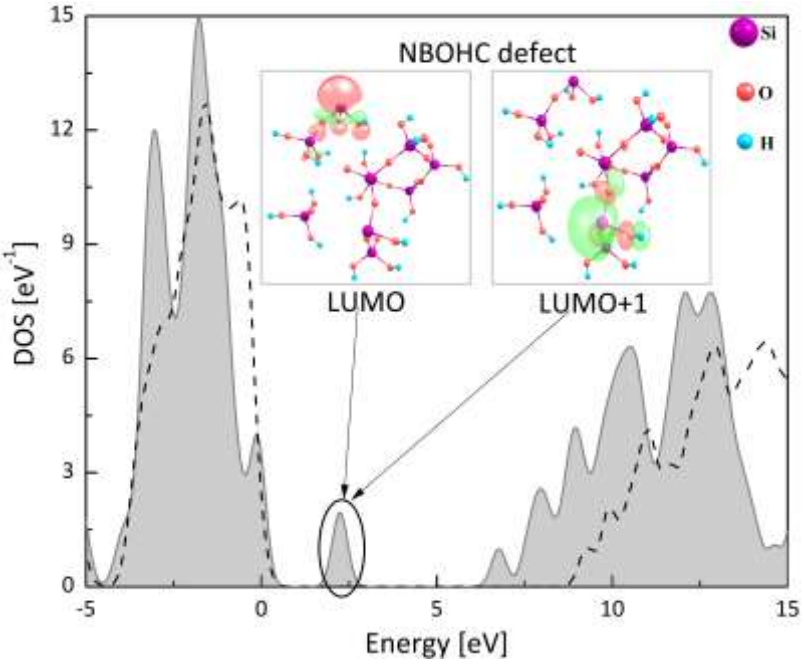

Figure 7. Electronic density of states at ground state (T_e = 0) (black dashed line) and just above the stability threshold (T_e = 2.805 eV) (gray-filled area) for $(SiO_2)_{10}$. The nonbridging oxygen hole center (NBOHC) defect is indicated by a black circle with corresponding molecular orbitals (LUMO and LUMO+1) (contour value σ = 0.2 Å^{-3}).

The nature of the peak for medium-basis-set DOS was revealed through the analysis of the composition and shape of molecular orbitals. It originates from two orbitals (LUMO and LUMO+1) corresponding to the edge of CB (**Figure7**). After geometry optimization, the original $(SiO_2)_{10}$ cluster splits into three parts ($Si_2H_5O_6$, $Si_7H_{12}O_{20}$ and SiH_3O_4). LUMO comes from $Si_2H_5O_6$ part and LUMO+1 comes mainly from the biggest part $Si_7H1_2O_{20}$ indicating that the peak in the bandgap region corresponds to the NBOHC defect formation. The defect is formed due to two broken Si-O bonds.[32] Obtaining an optimized structure with a defect in the case of the large basis set is not possible because the system is completely destroyed above the threshold. Together with the electronic and atomic rearrangement, the formation of defects in the structure is the reason for the bandgap collapse at higher value of T_e. Previously, photoexcited lattice distortions were shown to affect silica optical properties related to the generation of self-trapped excitons.[31, 32, 65, 72]

IV. Conclusion

In this work we analyzed the stability of the amorphous silica bandgap and structure at high densities of ultrafast photoexcited electrons, using FT-DFT. Our calculation approach successfully reconstructs molecular systems from several $(SiO_4)^{4-}$ tetrahedra to facilitate the modelling of bulk amorphous materials properties. Applied to fused silica glass, we found a good qualitative agreement between theoretical and experimental properties at ground state regarding all analyzed quantities, including the geometry parameters, namely bond length and angle, macroscopic density and bandgap for molecular cluster based on 10 orthosilicate anion tetrahedra. Responding to the instantaneous electron thermal excitation, maximum values of bond elongation (7%) and volume expansion (20%) were estimated. Remarkably, all changes occurring in the electronic and atomic structures lead to a bandgap narrowing. The bandgap decrease reaches 2.3 and 2.5 eV for large and medium basis sets respectively and 5 eV for small basis set. Large bandgap decrease observed for small basis set was associated with expected defect formation appeared in the DOS. Such bandgap modification will affect nonlinearly the photoexcitation, strongly impacting the fused silica optical response under intense ultrashort laser pulse.

At T_e higher than 2.5 eV the system loses its thermodynamical stability and breaks down. This temperature creates the excited electron density on the order of 10^{22} cm^{-3} which corresponds to around 4% of valence electrons transferred to the conduction band, comparable to the fused silica damage threshold reported experimentally.[73, 74] If the laser pulse excitation is sufficiently strong, interatomic forces are changed and the atoms start moving away from

the ground state positions. Consequently, the structure of the bulk material disorders within several hundreds of femtoseconds, with a processing time that can be controlled by the induced electron temperature and thus by the excitation level.[68] The physical mechanisms underlying the change in the band gap value of fused silica is attributed to atomic rearrangement and charge transfer between the Si and O atoms.

The presented results deliver a comprehensive understanding of the fundamental mechanisms of ultrashort laser-induced modification on the timescale comparable to the laser pulse duration. The outcome of this study is useful for defining the optimal laser parameters for material processing, for quantifying transient processes and finally for predicting the kinetics of matter movement and phase transformation upon ultrafast excitation.

Acknowledgements

The work was funded by IDEXLYON project of the University of Lyon within the program "Investissements d'Avenir"(ANR-16-IDEX-0005) and INTRALAS project (ANR-19-CE30-0036) operated by the French National Research Agency (ANR). The numerical calculations were performed using computer resources from GENCI, project gen7041.

Data availability

The data that support the table and findings of this study are available from the corresponding author upon reasonable request.

References

[1] M. Malinauskas *et al.*, Light-Science & Applications **5**, e16133 (2016) 14.
[2] M. Ams *et al.*, Nanophotonics **6** (2017) 743.
[3] S. Nolte *et al.*, Applied Physics a-Materials Science & Processing **77** (2003) 109.
[4] J. Y. Zhang *et al.*, Physical Review Letters **112**, 033901 (2014) 5.
[5] A. Rodenas *et al.*, Nature Photonics **13** (2019) 105.
[6] T. T. Fernandez *et al.*, Progress in Materials Science **94** (2018) 68.
[7] D. G. MacLachlan *et al.*, Monthly Notices of the Royal Astronomical Society **464** (2017) 4950.
[8] R. Stoian, Applied Physics a-Materials Science & Processing **126**, 438 (2020) 30.
[9] L. Sansoni *et al.*, Physical Review Letters **105**, 200503 (2010) 4.
[10] D. N. Biggerstaff *et al.*, Nature Communications **7**, 11282 (2016) 6.
[11] H. J. Wang *et al.*, Laser & Photonics Reviews, 2100563 7.
[12] M. Schultze *et al.*, Nature **493** (2013) 75.
[13] A. Sommer *et al.*, Nature **534** (2016) 86.
[14] F. J. Furch *et al.*, Optics Letters **44** (2019) 4267.
[15] A. Rudenko *et al.*, Advanced Optical Materials **9**, 2100973 (2021) 9.
[16] Y. Yacoby, Physical Review **169** (1968) 610.
[17] M. Lucchini *et al.*, Science **353** (2016) 916.

[18] F. Walter, Zeitschrift fur Naturforschung - Section A Journal of Physical Sciences **13** (1958) 484.
[19] L.V. Keldysh, Soviet Physics JETP (USSR) **7**, 075102 (1958) 788.
[20] F. Novelli *et al.*, Scientific Reports **3**, 1227 (2013) 5.
[21] C. R. McDonald, A. Ben Taher, and T. Brabec, Journal of Optics **19**, 114005 (2017) 10.
[22] K. Sokolowski-Tinten, and D. von der Linde, Physical Review B **61** (2000) 2643.
[23] P. Stampfli, and K. H. Bennemann, Physical Review B **42** (1990) 7163.
[24] M. Schultze *et al.*, Science **346** (2014) 1348.
[25] T. Winkler *et al.*, Nature Physics **14** (2018) 74.
[26] S. Minomura, and H. G. Drickamer, Journal of Physics and Chemistry of Solids **23** (1962) 451.
[27] R. H. Wentorf Jr, and J. S. Kasper, Science **139** (1963) 338.
[28] T. Dumitrica, and R. E. Allen, Physical Review B **66**, 081202 (2002) 4.
[29] S. A. Sato *et al.*, Physical Review B **92**, 205413 (2015) 6.
[30] G. Pacchioni, A. M. Ferrari, and G. Ierano, Faraday Discussions **106** (1997) 155.
[31] N. L. Anderson *et al.*, Physical Review Letters **106** (2011)
[32] R. M. Van Ginhoven *et al.*, Journal of Chemical Physics **118** (2003) 6582.
[33] K. L. Yip, and W. B. Fowler, Physical Review B **10** (1974) 1400.
[34] Y. Hirokawa *et al.*, International Journal of High Performance Computing Applications, 10943420211065723 16.
[35] F. Neese, Wiley Interdisciplinary Reviews-Computational Molecular Science **8**, e1327 (2018) 6.
[36] C. A. Bauer, A. Hansen, and S. Grimme, Chemistry-a European Journal **23** (2017) 6150.
[37] A. D. Becke, Journal of Chemical Physics **98** (1993) 5648.
[38] R. Krishnan *et al.*, Journal of Chemical Physics **72** (1980) 650.
[39] E. Silla, I. Tunon, and J. L. Pascualahuir, Journal of Computational Chemistry **12** (1991) 1077.
[40] S. Grimme, and A. Hansen, Angewandte Chemie-International Edition **54** (2015) 12308.
[41] N. S. Ostlund, A. Szaboa, Modern Quantum Chemistry: Introduction to Advanced Electronic Structure Theory (Dover Publications; Reprint Edition, 1996).
[42] M. Noda *et al.*, Computer Physics Communications **235** (2019) 356.
[43] A. Yamada, and K. Yabana, European Physical Journal D **73**, 87 (2019) 9.
[44] K. M. Lee *et al.*, Journal of Applied Physics **115**, 053519 (2014) 8.
[45] F. Pio *et al.*, Physica Status Solidi B-Basic Research **159** (1990) 577.
[46] G. Pacchioni, and M. Vitiello, Journal of Non-Crystalline Solids **245** (1999) 175.
[47] G. Pacchioni, and G. Ierano, Journal of Non-Crystalline Solids **216** (1997) 1.
[48] G. Pacchioni, and G. Ierano, Physical Review B **56** (1997) 7304.
[49] A. Rimola *et al.*, Chemical Reviews **113** (2013) 4216.
[50] J. Sauer *et al.*, Chemical Reviews **94** (1994) 2095.
[51] R. M. Van Ginhoven, H. Jonsson, and L. R. Corrales, Physical Review B **71**, 024208 (2005) 15.
[52] T. H. DiStefano, and D. E. Eastman, Solid State Communications **9** (1971) 2259.
[53] J. L. Bredas, Materials Horizons **1** (2014) 17.
[54] J. Paier *et al.*, Journal of Chemical Physics **124**, 154709 (2006) 13.
[55] J. Heyd *et al.*, Journal of Chemical Physics **123**, 174101 (2005) 8.
[56] A. A. Tsaturyan, A. P. Budnyk, and C. Ramalingan, ACS Omega **4** (2019) 10991.
[57] B. Lim, X. Y. Cui, and S. P. Ringer, Physical Chemistry Chemical Physics **23** (2021) 5407.
[58] C. Rostgaard, K. W. Jacobsen, and K. S. Thygesen, Physical Review B **81**, 085103 (2010) 10.
[59] S. Sen, and J. E. Dickinson, Physical Review B **68**, 214204 (2003) 6.

[60] Y. N. Xu, and W. Y. Ching, Physical Review B **44** (1991) 11048.
[61] E. Guler *et al.*, Chinese Journal of Physics **65** (2020) 472.
[62] E. Bevillon *et al.*, Physical Review B **89**, 115117 (2014) 11.
[63] M. Uemoto *et al.*, Journal of Chemical Physics **150**, 094101 (2019) 11.
[64] R. L. Mozzi, and B. E. Warren, Journal of Applied Crystallography **2** (1969) 164.
[65] R.M. Van Ginhoven, H. Jonsson., L. R. Corrales, Journal of Non-Crystalline Solids **352** (2006) 2589.
[66] R. S. Mulliken, The Journal of Chemical Physics **23** (1955) 1833.
[67] L. Ben-Mahfoud *et al.*, Physical Review B **104**, 104104 (2021) 10.
[68] T. Zier, E. S. Zijlstra, and M. E. Garcia, Applied Physics a-Materials Science & Processing **117** (2014) 1.
[69] R. A. Voronkov *et al.*, Nuclear Instruments & Methods in Physics Research Section B-Beam Interactions with Materials and Atoms **435** (2018) 87.
[70] B. Bauerhenne, and M. E. Garcia, Advanced Optical Technologies **9** (2020) 145.
[71] S. V. Faleev *et al.*, Physical Review B **74**, 033101 (2006) 4.
[72] T.E. Tsai, and D. L. Griscom, Physical Review Letters **67** (1991) 2517.
[73] J. Huang *et al.*, Scientific Reports **7**, 16239 (2017) 12.
[74] G. D. Tsibidis, and E. Stratakis, Scientific Reports **10**, 8675 (2020) 13.